

Model predictive control of ITER plasma current and shape using singular-value decomposition

Samo Gerkšič^a, Boštjan Pregelj^a, Matija Perne^a, Marco Ariola^b, Gianmaria De Tommasi^c and Alfredo Pironi^c

^a *Jozef Stefan Institute, Jamova cesta 39, 1000 Ljubljana, Slovenia*

^b *Consorzio CREATE / Università di Napoli Parthenope, Dipartimento di Ingegneria, Centro Direzionale di Napoli, isola C4, 80143 Napoli, Italy*

^c *Consorzio CREATE / Università di Napoli Federico II, Dipartimento di Ingegneria Elettrica e delle Tecnologie dell'informazione, Via Claudio 21, 80125 Napoli, Italy*

A model predictive control (MPC) scheme for ITER plasma current and shape controller (PCSC) is presented. The controller is able to control a large number of geometrical plasma shape descriptors using output-space reduction based on singular-value decomposition (SVD). The online optimisation problems imposed by MPC are solved using the dual fast gradient method (dFGM) solver, which is shown to be computationally feasible when MPC complexity-reduction techniques are applied. A performance evaluation in simulation of the flat-top phase of ITER Scenario 1 is presented, showing a moderate general improvement of control, compared to a reference control scheme based on multivariable PID control with SVD. Moreover, the proposed MPC PCSC is capable of avoiding superconductive current saturations, and in some cases shows better performance regarding voltage saturations.

Keywords: predictive control, plasma magnetic control, quadratic programming, singular value decomposition.

1. Introduction

In a magnetically confined tokamak reactor, the Plasma Current and Shape Controller (PCSC) is in charge of driving the voltages applied to the poloidal field coils, in order to control plasma shape, current, and position. In most cases, such as the ITER tokamak, the PCSC is designed taking into account the presence of the Vertical Stabilisation controller. The challenge of PCSC is to maintain the prescribed plasma shape and distance from the plasma facing components, in presence of specific disturbances, such as H-L transitions or edge-localised modes (ELM), during the various phases of the discharge.

Model Predictive Control (MPC) [1] has gained wide industrial acceptance by facilitating a systematic approach to control of large-scale multivariable systems, with efficient handling of constraints on process variables and enabling plant optimization. With linear-model-based MPC, on-line quadratic programming (QP) optimization problems are being solved repeatedly at each sample time of the PCSC control loop for determining control actions. The computation time used to be the main obstacle for applying MPC to complex multivariable control problems with fast dynamics. Recently, a new generation of fast QP solvers for use with MPC has been conceived, based on active-set [2], interior-point [3] and first-order approaches [4, 5], initially demonstrated on small-scale examples.

A simulation evaluation of an MPC approach to tokamak control at the plasma physics level was described in [6] for the Tore Supra, in [7] for the DIII-D, and in [8] for the NSTX-U. Related work [9] uses online QP in a reference-governor approach to ITER PCSC. A practical-scale fast MPC controller was demonstrated for ITER safety factor profile control [10], reaching QP

computation times under 8 ms with hard input and soft state constraints using an active-set type QP solver; an MPC controller was tested experimentally on the TCV tokamak [11] reaching computation times under 0.3 ms with hard input constraints only. Another recent experimental study on the DIII-D [12] reports average computation times around 1 ms with input constraints only. Our preliminary work [13] has already shown that MPC control is computationally feasible for a prototype implementation of ITER PCSC, using a dual fast gradient method (dFGM) solver [5] and complexity-reduction techniques, with computation times below 7 ms when applying hard input and soft state constraints.

In this work we present an MPC PCSC for the flat-top phase of ITER Scenario 1, which is able to control a large number of geometrical plasma shape descriptors using output-space reduction based on singular-value decomposition (SVD). Aside for the input restrictions of poloidal-field voltages, the controller is capable of avoiding poloidal-field current saturations, considered via soft constraints on the system states. A similar SVD-based approach was previously applied in the reference control scheme [14,15], which is based on multivariable PI control. A performance evaluation that compares the two control approaches in simulation is given.

2. Plasma magnetic control and models

The simulations and controller design methods are based on high-order local linear dynamical models of the tokamak plasma from CREATE-L or CREATE-NL [16, 17] nonlinear equilibrium codes, at several different operating points for ITER plasma Scenario 1. The most important models are listed in Table 1. The model codes coincide with the time into the scenario.

Table 1. Local linear dynamic models.

Model code	ITER Scenario 1 time (s)	Growth rate (s ⁻¹)
t080	80	9.1
t090	90	3.6
t520	520	2.9

The Matlab/Simulink simulation scheme comprises:

- the plasma/circuits linearized model,
- sum nodes to append the operating-point offset to the outputs of the plasma linear model, in order to generate "nominal" signal values,
- a simplified model of plasma diagnostics for the plasma vertical velocity v_p and position z_p (a first-order dynamic lag filter with the time constant equal to $7 \cdot 10^{-3}$ s is considered),
- simplified models of the power supplies for the superconductive (SC) coils VS1 and for the in-vessel ohmic coils VS3 (a first-order dynamic lag with the time constant equal to $7.5 \cdot 10^{-3}$ s; a delay equal to $2.5 \cdot 10^{-3}$ s; saturations ± 6 kV and ± 1.5 kV for VS1 and VS3, respectively),
- simplified models of the main power supplies (saturations ± 1.5 kV, except for VCS1 ± 3 kV, and first-order dynamic lag with the time constant equal to 0.015 s and a delay equal to 0.015 s),
- the inner cascade control loop of the vertical stabilisation (VS) system, which aims at vertically stabilising the plasma column,
- the outer cascade control loop of the PCSC, which controls plasma current and shape,
- blocks enabling the simulation of a vertical displacement event (VDE), using a corresponding plasma model initial state, and minor disruption, uncontrolled ELM, L-H & H-L transitions, by injecting recorded profiles of poloidal beta β_p and internal inductance l_i [14].

2.1 Vertical Stabilisation

For VS, an approach similar to the one proposed in [14] is used both in the reference scheme and with the MPC controller.

The VS controller acts on the control variable $\mathbf{u}_{VS} = [u_{VS,1} \ u_{VS,2}]^T$, where:

- $u_{VS,1}$ is the voltage applied to the in-vessel coils VS3,
- $u_{VS,2}$ is the voltage applied to the SC circuit VS1,

while it attempts to drive to zero the controlled inputs $\mathbf{y}_{VS} = [y_{VS,1} \ y_{VS,2}]^T$, where

- $y_{VS,1}$ is the VS3 power supply current,
- $y_{VS,2}$ is the plasma vertical velocity v_p .

The following feedback transfer function matrix is used for the V controller

$$\mathbf{u}_{VS}(t) = \mathbf{K}_{\text{SOF}} \mathbf{y}_{VS}(t), \quad (1)$$

$$\mathbf{K}_{\text{SOF}} = \begin{bmatrix} \frac{0.00175s + 0.07}{(1/6)s + 1} & -\frac{175s + 7000}{(1/6)s + 1} \\ 0.1 & 0 \end{bmatrix}$$

3. Basic MPC plasma current and shape controller

The manipulated variables (output vector \mathbf{u}_{CSC}) of the PCSC are the 11 main power supply voltages in the \mathbf{V}_{PF} vector.

The controlled variables (measurement vector \mathbf{y}_{CSC}) of the PCSC include:

- the currents in the 11 SC coils \mathbf{I}_{PF} ,
- the plasma current I_p ,
- the vector of 29 geometrical descriptors \mathbf{g} , comprising gaps and two strike-points.

MPC PCSC design starts by preparing the nominal model, starting from the model t090 with plasma resistance set to 0. The simplified models of the power supplies and sensors (diagnostics) are appended. Then, the VS feedback loop is added, and the subsystem from the process inputs $\mathbf{u}_{\text{CSC}} = \mathbf{V}_{\text{PF}}$ to the outputs $\mathbf{y}_{\text{CSC}} = [\mathbf{I}_{\text{PF}}^T \ I_p^T \ \mathbf{g}^T]^T$ is extracted. Using Hankel balanced truncation, the order of the subsystem is reduced from 207 to 60. Finally, the base model for the MPC PCSC $\{\mathbf{A}_{\text{CSC}}, \mathbf{B}_{\text{CSC}}, \mathbf{C}_{\text{CSC}}, \mathbf{0}\}$ is obtained with model conversion to discrete time with the sampling time $T_s = 0.1$ s, assuming zero-order hold.

The PCSC should facilitate offset-free control of I_p and \mathbf{g} with integral action. In our implementation, integral action is based on the *disturbance estimation* (DE) concept [18], and the *velocity form* is used to prevent offset due to the control cost when the control signal is non-zero at the steady-state.

For the estimation of asymptotically non-zero disturbances, the base model is augmented with DE integrators at the outputs which require offset-free control. Consider the discrete-time state-space model

$$\begin{aligned} \mathbf{x}(k+1) &= \mathbf{A}\mathbf{x}(k) + \mathbf{B}\mathbf{u}(k) + \mathbf{w}(k), \\ \mathbf{y}(k) &= \mathbf{C}\mathbf{x}(k) + \mathbf{v}(k) \end{aligned} \quad (2)$$

where \mathbf{w} and \mathbf{v} are white noise signals to the state and output, respectively. DE integrator states \mathbf{d} with the associated white-noise signal \mathbf{w}_d are appended to the state \mathbf{x} , so that the augmented state is $\mathbf{x}_a = [\mathbf{x}^T \ \mathbf{d}^T]^T$, and $\mathbf{w}_a = [\mathbf{w}^T \ \mathbf{w}_d^T]^T$. The augmented system is

$$\begin{aligned} \begin{bmatrix} \mathbf{x}(k+1) \\ \mathbf{d}(k+1) \end{bmatrix} &= \begin{bmatrix} \mathbf{A} & \mathbf{0} \\ \mathbf{0} & \mathbf{I} \end{bmatrix} \begin{bmatrix} \mathbf{x}(k) \\ \mathbf{d}(k) \end{bmatrix} + \begin{bmatrix} \mathbf{B} \\ \mathbf{0} \end{bmatrix} \mathbf{u}(k) + \begin{bmatrix} \mathbf{I} & \mathbf{0} \\ \mathbf{0} & \mathbf{I} \end{bmatrix} \begin{bmatrix} \mathbf{w}(k) \\ \mathbf{w}_d(k) \end{bmatrix} \\ \mathbf{y}(k) &= [\mathbf{C} \ \mathbf{I}] \begin{bmatrix} \mathbf{x}(k) \\ \mathbf{d}(k) \end{bmatrix} + \mathbf{v}(k) \end{aligned} \quad (3)$$

and is rewritten as

$$\begin{aligned} \mathbf{x}_a(k+1) &= \mathbf{A}_a \mathbf{x}_a(k) + \mathbf{B}_a \mathbf{u}_a(k) + \mathbf{w}_a(k), \\ \mathbf{y}(k) &= \mathbf{C}_a \mathbf{x}_a(k) + \mathbf{v}(k) \end{aligned} \quad (4)$$

The steady-state Kalman filter (KF)

$$\begin{aligned} \mathbf{x}_a(k/k-1) &= \mathbf{A}_a \mathbf{x}_a(k-1/k-1) + \mathbf{B}_a \mathbf{u}(k-1) \\ \mathbf{x}_a(k/k) &= \mathbf{x}_a(k/k-1) + \mathbf{M}_K [\mathbf{y}(k) - \mathbf{C}_a \mathbf{x}_a(k/k-1)] \end{aligned} \quad (5)$$

is used for state estimation with the disturbance-augmented model, where \mathbf{M}_K is computed via the steady-state solution of the Riccati equation from the covariance matrices $\mathbf{Q}_K = \mathbf{E}\{\mathbf{w}_a \mathbf{w}_a^T\}$ and $\mathbf{R}_K = \mathbf{E}\{\mathbf{v} \mathbf{v}^T\}$. The KF is used in the sense of an observer, where the diagonal elements

of \mathbf{Q}_K and \mathbf{R}_K are used as tuning parameters to achieve desired dynamics.

For the velocity form, the disturbance-augmented system $\{\mathbf{A}_a, \mathbf{B}_a, \mathbf{C}_a, \mathbf{0}\}$ is augmented again. In the velocity-augmentation, the change of the input signal $\delta\mathbf{u}$ becomes the new input; the state expands to $\mathbf{x}_{av} = [\mathbf{x}_a^T \mathbf{u}(k-1)^T]^T$; the new output is $\mathbf{y}_{av} = [\mathbf{y}_a^T \mathbf{u}(k-1)^T]^T$

$$\begin{aligned} \begin{bmatrix} \mathbf{x}_a(k+1) \\ \mathbf{u}(k) \end{bmatrix} &= \begin{bmatrix} \mathbf{A}_a & \mathbf{B}_a \\ \mathbf{0} & \mathbf{I} \end{bmatrix} \begin{bmatrix} \mathbf{x}_a(k) \\ \mathbf{u}(k-1) \end{bmatrix} + \begin{bmatrix} \mathbf{B}_a \\ \mathbf{I} \end{bmatrix} \delta\mathbf{u}(k) \\ \begin{bmatrix} \mathbf{y}_a(k) \\ \mathbf{u}(k-1) \end{bmatrix} &= \begin{bmatrix} \mathbf{C}_a & \mathbf{D}_a \\ \mathbf{0} & \mathbf{I} \end{bmatrix} \begin{bmatrix} \mathbf{x}_a(k) \\ \mathbf{u}(k-1) \end{bmatrix} + \begin{bmatrix} \mathbf{D}_a \\ \mathbf{0} \end{bmatrix} \delta\mathbf{u}(k) \end{aligned} \quad (6)$$

with $\mathbf{D}_a = \mathbf{0}$ rewritten as

$$\begin{aligned} \mathbf{x}_{av}(k+1) &= \mathbf{A}_{av} \mathbf{x}_{av}(k) + \mathbf{B}_{av} \delta\mathbf{u}(k) \\ \mathbf{y}_{av}(k) &= \mathbf{C}_{av} \mathbf{x}_{av}(k) \end{aligned} \quad (7)$$

Then, the MPC controller is built in the output-cost formulation, with the cost function

$$\begin{aligned} J(\delta\tilde{\mathbf{u}}) &= \sum_{k=0}^{N-1} (\mathbf{y}_{av,k}^T \begin{bmatrix} \mathbf{Q}_{C,y} & \mathbf{0} \\ \mathbf{0} & \mathbf{0} \end{bmatrix} \mathbf{y}_{av,k} + \delta\tilde{\mathbf{u}}_k^T \mathbf{R}_{C,\delta\tilde{\mathbf{u}}} \delta\tilde{\mathbf{u}}_k + \\ &\quad + \mathbf{w}_s^T \mathbf{s}_k + \mathbf{s}_k^T \mathbf{W}_s \mathbf{s}_k) \end{aligned} \quad (8)$$

where N is the prediction horizon length, $\mathbf{Q}_{C,y}$ and $\mathbf{R}_{C,\delta\tilde{\mathbf{u}}}$ are diagonal cost matrices for the outputs and the control moves, respectively, \mathbf{s} is the vector of slack variables associated with soft constraints, \mathbf{w}_s is the linear slack cost vector, and \mathbf{W}_s is the quadratic slack cost matrix (diagonal).

The control law is formulated by minimising J with respect to the vector of the future control moves $\delta\tilde{\mathbf{u}}$ subject to constraints (\mathbf{V}_{PF} as hard constraints $\mathbf{u}_{\min} \leq \mathbf{u} \leq \mathbf{u}_{\max}$; \mathbf{I}_{PF} as soft output constraints $\mathbf{y}_{\min} - \mathbf{s} \leq \mathbf{y} \leq \mathbf{y}_{\max} + \mathbf{s}$). The control law is reformulated as a QP problem and solved using the dFGM QP solver. It is applied in receding-horizon manner, meaning that only $\delta\mathbf{u}_0$ values are used for the computation of the controller output $\mathbf{u}(k)$, while the predicted values are discarded and recomputed in the following time-step.

Minimising the cost function in (8) drives the output \mathbf{y}_a towards zero, whereas the PCSC controller must drive the process output towards the reference values $\mathbf{y}_{CSC,ref} = [\mathbf{I}_{PF,ref}^T \mathbf{I}_{p,ref}^T \mathbf{g}_{ref}^T]^T$, defined by the plasma physics layer. Reference tracking is implemented by subtracting the reference values from the process output at the input of the PCSC block, then feeding the difference ($\mathbf{y}_{CSC,ref} - \mathbf{y}_{CSC}$) instead of \mathbf{y}_{CSC} to the input of the KF. A similar subtraction must be applied to the output constraints (rendering their limit values reference-dependent).

The horizon $N = 30$ is used. To reduce the computational demand, the number of free future control moves is reduced from 30 to 3 using move blocking to intervals [2 2 26]. An additional efficient complexity-reduction method is to impose output constraints only at each third sample of the prediction horizon.

4. SVD-based PCSC

The basic version of the MPC PCSC controller in the previous section uses the full output vector \mathbf{y} including the vector \mathbf{g} with 29 geometrical descriptors. When the controlled system has many more controlled outputs than manipulated variables, offset-free performance in the steady state is not possible, there may be issues in tuning, and the model is undesirably large.

The controller complexity may be reduced by selecting \mathbf{g}_{sel} as a smaller subset of elements of \mathbf{g} . One may also choose to control weighted sums of adjacent gaps, rather than selecting individual gaps. This may be specified by introducing an appropriate output selection matrix \mathbf{M}_{sel}

$$\mathbf{g}_{sel} = \mathbf{M}_{sel} \mathbf{g} \quad (9)$$

Subsequently, the controller is designed for the output vector $\mathbf{y}_{CSCsel} = [\mathbf{I}_{PF}^T \mathbf{I}_p^T \mathbf{g}_{sel}^T]^T$ instead of the original output vector $\mathbf{y}_{CSC} = [\mathbf{I}_{PF}^T \mathbf{I}_p^T \mathbf{g}^T]^T$. In the base model $\{\mathbf{A}_{CSC}, \mathbf{B}_{CSC}, \mathbf{C}_{CSC}, \mathbf{0}\}$, the matrix \mathbf{C}_{CSC} is replaced with a reduced matrix \mathbf{C}_{CSCsel} , which only retains rows corresponding to the gaps selected in \mathbf{g}_{sel} (or averaged rows for the weighted sums).

Instead of selecting outputs manually, one may reduce the output dimension considering the steady-state relation between \mathbf{I}_{PF} and \mathbf{g} using SVD as in [14], where the aim is to achieve a minimum weighted tracking error $(\mathbf{g} - \mathbf{g}_{ref})^T \mathbf{Q}_{SVD} (\mathbf{g} - \mathbf{g}_{ref})$ in the steady state, while also striving towards low control effort $(\mathbf{I}_{PF} - \mathbf{I}_{PF,ref})^T \mathbf{R}_{SVD} (\mathbf{I}_{PF} - \mathbf{I}_{PF,ref})$ in the steady state. Here, \mathbf{Q}_{SVD} and \mathbf{R}_{SVD} are diagonal weighting matrices, by default identity matrices, but they may be altered to tune steady-state offsets of particular elements of \mathbf{g} and \mathbf{I}_{PF} .

With this approach, the model must be rearranged so that the matrix \mathbf{C}_g , which is to be decomposed using SVD, contains the steady-state relation between \mathbf{I}_{PF} and \mathbf{g} . The base model $\{\mathbf{A}_{CSC}, \mathbf{B}_{CSC}, \mathbf{C}_{CSC}, \mathbf{0}\}$ undergoes a state-space transformation to an input-to-output equivalent form $\{\mathbf{A}_{CSCt}, \mathbf{B}_{CSCt}, \mathbf{C}_{CSCt}, \mathbf{0}\}$ in which \mathbf{I}_{PF} appears explicitly in the state vector. In this transformed form, the relation between the states including \mathbf{I}_{PF} and the \mathbf{I}_{PF} outputs is an identity matrix, and the relation between the states including \mathbf{I}_{PF} and the output \mathbf{g} is the sought \mathbf{C}_g matrix.

\mathbf{C}_g could be decomposed using SVD, in the basic form

$$\mathbf{C}_g = \mathbf{U}_0 \mathbf{S}_0 \mathbf{V}_0^T \quad (10)$$

however, actually, the weighted form is used

$$\tilde{\mathbf{C}}_g = \mathbf{Q}_{SVD}^{\frac{1}{2}} \mathbf{C}_g \mathbf{R}_{SVD}^{\frac{1}{2}} = \mathbf{U}_0 \mathbf{S}_0 \mathbf{V}_0^T \quad (11)$$

A truncated SVD approximation using the first n_g singular values is

$$\tilde{\mathbf{C}}_{g1} = \mathbf{Q}_{SVD}^{\frac{1}{2}} \mathbf{C}_{g1} \mathbf{R}_{SVD}^{\frac{1}{2}} = \mathbf{U}_1 \mathbf{S}_1 \mathbf{V}_1^T \quad (12)$$

or

$$\mathbf{C}_{g1} = \mathbf{Q}_{SVD}^{\frac{1}{2}} \mathbf{U}_1 \mathbf{S}_1 \mathbf{V}_1^T \mathbf{R}_{SVD}^{\frac{1}{2}} \quad (13)$$

The artificial gaps vector \mathbf{g}_{SVD} with reduced dimension n_g is introduced so that

$$\mathbf{g} = \mathbf{Q}_{\text{SVD}}^{-\frac{1}{2}} \mathbf{U}_1 \mathbf{g}_{\text{SVD}} \quad (14)$$

The controller is designed for the output vector $\mathbf{y}_{\text{CSC,SVD}} = [\mathbf{I}_{\text{PF}}^T I_p^T \mathbf{g}_{\text{SVD}}^T]^T$ instead of the original output vector $\mathbf{y}_{\text{CSC}} = [\mathbf{I}_{\text{PF}}^T I_p^T \mathbf{g}^T]^T$. The simulation scheme in Fig. 1 is used, with the MPC PCSC block expanded in Fig. 2. The mapping from \mathbf{g} to \mathbf{g}_{SVD} , in place of \mathbf{M}_{sel} to form the system state-space model with the artificial output, is

$$\mathbf{g}_{\text{SVD}} = (\mathbf{U}_1^T \mathbf{U}_1)^{-1} \mathbf{U}_1^T \mathbf{Q}_{\text{SVD}}^{\frac{1}{2}} \mathbf{g} \quad (15)$$

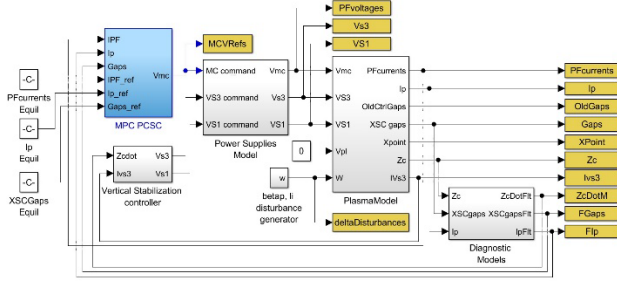


Fig. 1. SVD-based MPC PCSC control scheme.

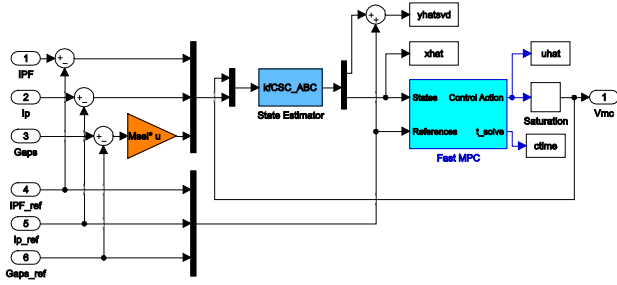


Fig. 2. MPC PCSC block expanded.

5. Reference PCSC scheme

For comparison, the PCSC algorithm CREATE v2d0 (see in [15]) is used. It implements a multivariable proportional-integral control law from \mathbf{g} and I_p , with an additional proportional contribution from \mathbf{I}_{PF} . It also includes windup protection in case of actuator saturation.

6. Performance evaluation

The control performance of the SVD-based MPC PCSC and the reference CREATE v2d0 scheme has been tested with local linear models from three operating points of the ITER Scenario 1: $t = 80$ s, $t = 90$ s and $t = 520$ s, considering five disturbance types (Minor Disruption, Uncontrolled ELM, L-H Transition, H-L Transition, Vertical Displacement Event), in total 36 experiments per controller (all combinations are not applicable).

Table 2 shows an overview of the essential control performance measures, which are formulated to capture the important information from the simulation data (much more detailed data is required for controller tuning and

detailed performance evaluation). The following performance measures are shown:

- **max(abs(dGaps))** - maximal gap displacement from the reference,
- **sum(abs(dGaps(end)))** - sum of gap displacements at the end of simulation,
- **avg(RISE(dGaps))** - average RISE¹ value of all gap displacements,
- **min(Gaps)** - the smallest gap of the plasma shape to the vessel wall during simulation,
- **max(dI_p)** - maximal plasma current displacement δI_p ,
- **RISE(dI_p)** - RISE value of δI_p ,
- **min(I_{PF}thresh - I_{PF})** - displacement of the closest \mathbf{I}_{PF} from its bound,
- **sum(abs(I_{PF}(end) - I_{PF}equi))** - sum of \mathbf{I}_{PF} displacements from the equilibrium value,
- **sum(RISE(dI_{PF}))** - sum of RISE of all \mathbf{I}_{PF} displacements from equilibrium,
- **max(abs(dI_{PF}))** - maximal \mathbf{I}_{PF} displacement from the equilibrium,
- **max(P_{tot})** - peak value of the total power consumption during simulation,
- **RISE(P_{tot})** - RISE value of the total power consumption for complete simulation,
- **sum(RISE(V_{PF}))** - sum of RISE of all \mathbf{V}_{PF} voltages.

In the simulations summarised in Table 2, SVD-based MPC PCSC generally shows better performance in terms of transient peak, settling time and the steady-state offset of gaps, and a much better performance in tracking of the plasma current than the reference scheme with most disturbances and local models. The $\min(\mathbf{I}_{\text{PF}}^{\text{thresh}} - \mathbf{I}_{\text{PF}})$ performance measure with model t520 reveals that the \mathbf{I}_{PF} current limits are violated with Minor Disturbance and H-L transition in case of the reference controller, while SVD-based MPC PCSC maintains control without limit violations. Fig. 3 displays a comparison of controlled signals of the two controllers in the most challenging case in the set with Minor Disturbance at $t = 520$ s. Due to the active \mathbf{I}_{PF} constraints of the coils CS2L and PF5 (top-right), the steady-state offsets of $\delta \mathbf{g}$ and δI_p are increased with the MPC PCSC controller. However, the transient $\delta \mathbf{g}$ and δI_p responses are handled much better than with the reference controller, which does also not respect the \mathbf{I}_{PF} constraints.

In the simulations, the SVD-based MPC PCSC was using a dFGM solver based on [5]. Peak iteration computation times under 3 ms and under 7 ms have been achieved with relative tolerances 10^{-3} and 10^{-4} , respectively, on a Linux system with a real-time kernel using an Intel Core i7-2600K -based computer.

7. Conclusions

An SVD-based MPC control scheme for ITER PCSC is presented. Its performance evaluation in simulation of specific disturbances in different operating points of the ITER Scenario 1 generally shows better performance in terms of transient peak, settling time and the steady-state offset of gaps, and a much better performance in tracking

¹ Root of Integral Square Error

of the plasma current than the reference scheme with most disturbances. Moreover, the proposed MPC PCSC is capable of avoiding superconductive current saturations, which is not the case with the reference scheme, and in some cases shows better performance regarding voltage saturations. The online optimisation of MPC QP problems is carried out using the dFGM method, with peak computation times under 7 ms.

Acknowledgments

Research supported by Slovenian Research Agency (P2-0001). This work has been carried out within the framework of the EUROfusion Consortium and has received funding from the Euratom research and training programme 2014-2018 under grant agreement No 633053. The views and opinions expressed herein do not necessarily reflect those of the European Commission.

References

[1] Qin S. J. and Badgwell T. A., "A survey of industrial model predictive control technology", *Control Eng. Pract.* **11**, 733–764 (2003).
 [2] Ferreau H. J. et al., "qpOASES, a parametric active-set algorithm for quadratic programming", *Math. Prog. Comp.* **6**, 327–363 (2014).
 [3] Mattingley J. and Boyd S., "CVXGEN: a code generator for embedded convex optimization", *Optim. Eng.* **13**, 1–27 (2012).
 [4] Hartley E. N. et al., "Predictive control using an FPGA with application to aircraft control", *IEEE Trans. Control Systems Technology*, **22**, 1006–1017 (2014).
 [5] Giselsson P., "Improving fast dual ascent for MPC - Part II: the embedded case", arXiv (2014).
 [6] Ouarit H. et al., "Validation of plasma current profile model predictive control in tokamaks via simulations", *Fus. Eng. Des.* **86**, 1018-1021 (2011).

[7] Ou et al., "Receding-horizon optimal control of the current profile evolution during the ramp-up phase of a tokamak discharge", *Con. Eng. Prac.* **19** 22-31 (2011).
 [8] Ilhan Z. et al., "Model predictive control with integral action for the rotational transform profile tracking in NSTX-U", *IEEE Multi-Conf. Sys. and Contr.*, Buenos Aires, Argentina, pp. 629-634 (2016).
 [9] Mattei M. et al., "A constrained control strategy for the shape control in thermonuclear fusion tokamaks", *Automatica* **49** 169-177 (2013).
 [10] Maljaars E., "Control of the tokamak safety factor profile with time-varying constraints using MPC", *Nucl. Fusion* **55** (2015).
 [11] Maljaars E., Model predictive profile control and actuator management in tokamaks, (PhD thesis, TU Eindhoven, 2017), section 4.
 [12] Wehner W. et al., "Predictive control of the tokamak q profile to facilitate reproducibility of high- q_{min} steady-state scenarios at DIII-D", *IEEE Multi-Conf. Sys. and Contr.*, Buenos Aires, Argentina, pp. 629-634 (2016).
 [13] Gerškic S., et al., "Plasma current and shape control for ITER using fast online MPC", 20th IEEE Real Time Conference, Padova (2016).
 [14] Ambrosino G. et al., "Design of the plasma position and shape control in the ITER tokamak using in-vessel coils," *IEEE Trans. Plasma Science*, 37(7) 1324-1331 (2009).
 [15] Ambrosino G. et al., "Design and nonlinear validation of the ITER magnetic control system," *IEEE Multi-Conf. Sys. and Contr.*, Sydney, Australia, pp. 1290-1295 (2015).
 [16] Albanese R. and Villone F., "The linearized CREATE-L plasma response model for the control of current, position and shape in tokamaks", *Nucl. Fus.* **38** (5) (1998).
 [17] Albanese R. et al., Plasma response models for current, shape and position control at JET, *Fusion Eng. Des.* **66–68** (2003).
 [18] Gerškic S. and Pregelj B., "Tuning of a tracking multi-parametric predictive controller using local linear analysis," *IET Control Theory Appl.* **6**, 1–11 (2012).

Table 2. Control performance evaluation measures overview for all relevant simulations.

	ctrl.	Plasma model t080					Plasma model t090				Plasma model t520			
		Minor Disruption	Uncontrolled ELM	LH transition	VDE	Minor Disruption	Uncontrolled ELM	HL transition	VDE	Minor Disruption	Uncontrolled ELM	HL transition	VDE	
<i>max(abs(dGaps))</i>	v2d0	0,208	0,021	0,161	0,274	0,234	0,025	0,149	0,234	0,428	0,052	0,178	0,235	
	FMPC	0,216	0,022	0,154	0,298	0,240	0,026	0,145	0,251	0,345	0,050	0,179	0,248	
<i>sum(abs(dGaps(end)))</i>	v2d0	0,126	0,026	0,115	0,000	0,189	0,046	0,084	0,000	0,399	0,116	0,297	0,000	
	FMPC	0,034	0,007	0,058	0,000	0,150	0,027	0,032	0,000	0,584	0,095	0,523	0,000	
<i>avg(RISE(dGaps))</i>	v2d0	0,161	0,017	0,171	0,010	0,202	0,019	0,170	0,014	0,369	0,043	0,178	0,015	
	FMPC	0,115	0,015	0,140	0,025	0,147	0,017	0,140	0,027	0,226	0,038	0,178	0,029	
<i>min(Gaps)</i>	v2d0	0,052	0,097	0,018	0,085	0,020	0,101	0,018	0,084	-0,018	0,093	0,024	0,081	
	FMPC	0,076	0,097	0,034	0,084	0,052	0,101	0,022	0,083	0,019	0,093	0,017	0,081	
<i>max(dIp)</i>	v2d0	3,03E+05	1,05E+04	1,57E+05	1,28E+05	3,05E+05	2,04E+04	1,91E+05	1,34E+05	5,49E+05	6,79E+04	1,32E+05	1,65E+05	
	FMPC	1,08E+05	1,05E+04	5,12E+04	1,37E+05	1,00E+05	1,19E+04	6,86E+04	1,42E+05	1,49E+05	6,07E+04	7,61E+04	1,71E+05	
<i>RISE(dIp)</i>	v2d0	5,51E+05	9,75E+03	2,80E+05	2,65E+04	6,13E+05	4,14E+04	3,27E+05	3,74E+04	9,66E+05	1,30E+05	2,02E+05	5,35E+04	
	FMPC	8,40E+04	5,64E+03	4,56E+04	5,13E+04	8,66E+04	8,79E+03	6,17E+04	5,89E+04	1,67E+05	3,27E+04	6,79E+04	7,73E+04	
<i>min(IPFthresh- IPF)</i>	v2d0	3,51E+03	2,00E+03	3,53E+03	3,52E+03	1,81E+03	3,50E+03	1,33E+03	3,46E+03	-1,78E+04	1,65E+03	-4,59E+03	3,83E+03	
	FMPC	3,41E+03	1,98E+03	3,53E+03	3,49E+03	4,94E+02	3,50E+03	1,21E+03	2,86E+03	2,28E+02	2,00E+02	2,13E+02	3,72E+03	
<i>sum(abs(IPF(end) - IPFeq))</i>	v2d0	7,80E+04	2,22E+04	1,06E+05	5,54E+00	1,02E+05	2,77E+04	6,39E+04	1,16E+01	1,41E+05	4,19E+04	1,09E+05	2,22E+01	
	FMPC	6,18E+04	1,77E+04	8,31E+04	2,31E+01	1,04E+05	2,56E+04	4,80E+04	2,99E+01	1,23E+05	6,74E+04	1,61E+05	3,87E+01	
<i>sum(RISE(dIPF))</i>	v2d0	4,15E+05	1,14E+05	5,29E+05	7,24E+02	5,24E+05	1,41E+05	3,13E+05	1,12E+03	7,50E+05	2,17E+05	5,39E+05	1,50E+03	
	FMPC	3,48E+05	9,14E+04	4,14E+05	1,05E+04	5,21E+05	1,30E+05	2,37E+05	9,73E+03	6,05E+05	3,43E+05	6,74E+05	1,10E+04	
<i>max(RISE(dIPF))</i>	v2d0	1,90E+04	4,51E+03	2,27E+04	7,83E+02	2,30E+04	5,60E+03	1,38E+04	1,10E+03	3,71E+04	9,07E+03	2,39E+04	1,19E+03	
	FMPC	1,45E+04	3,94E+03	2,07E+04	1,23E+03	2,20E+04	5,42E+03	1,24E+04	1,47E+03	2,88E+04	1,57E+04	3,94E+04	1,77E+03	
<i>max(Ptot)</i>	v2d0	1,77E+08	1,84E+07	9,86E+07	1,19E+08	2,30E+08	3,48E+07	3,26E+07	1,80E+08	4,37E+08	1,29E+08	1,10E+08	2,01E+08	
	FMPC	1,95E+08	1,33E+07	1,54E+08	7,75E+07	2,34E+08	1,78E+07	1,02E+08	1,38E+08	2,64E+08	7,43E+07	1,67E+08	2,20E+08	
<i>RISE(Ptot)</i>	v2d0	3,08E+08	1,33E+07	2,13E+08	1,91E+07	3,97E+08	3,20E+07	5,34E+07	3,98E+07	1,02E+09	1,33E+08	1,37E+08	4,80E+07	
	FMPC	2,72E+08	2,50E+07	2,62E+08	5,57E+07	3,23E+08	3,21E+07	1,15E+08	8,15E+07	4,15E+08	1,17E+08	4,16E+08	1,20E+08	
<i>sum(RISE(VPF))</i>	v2d0	3,41E+04	6,80E+03	2,68E+04	2,47E+03	3,61E+04	8,32E+03	1,59E+04	3,77E+03	5,85E+04	1,48E+04	2,69E+04	4,50E+03	
	FMPC	3,29E+04	6,69E+03	2,73E+04	1,38E+04	3,33E+04	8,13E+03	1,75E+04	1,39E+04	4,24E+04	1,96E+04	5,32E+04	1,29E+04	

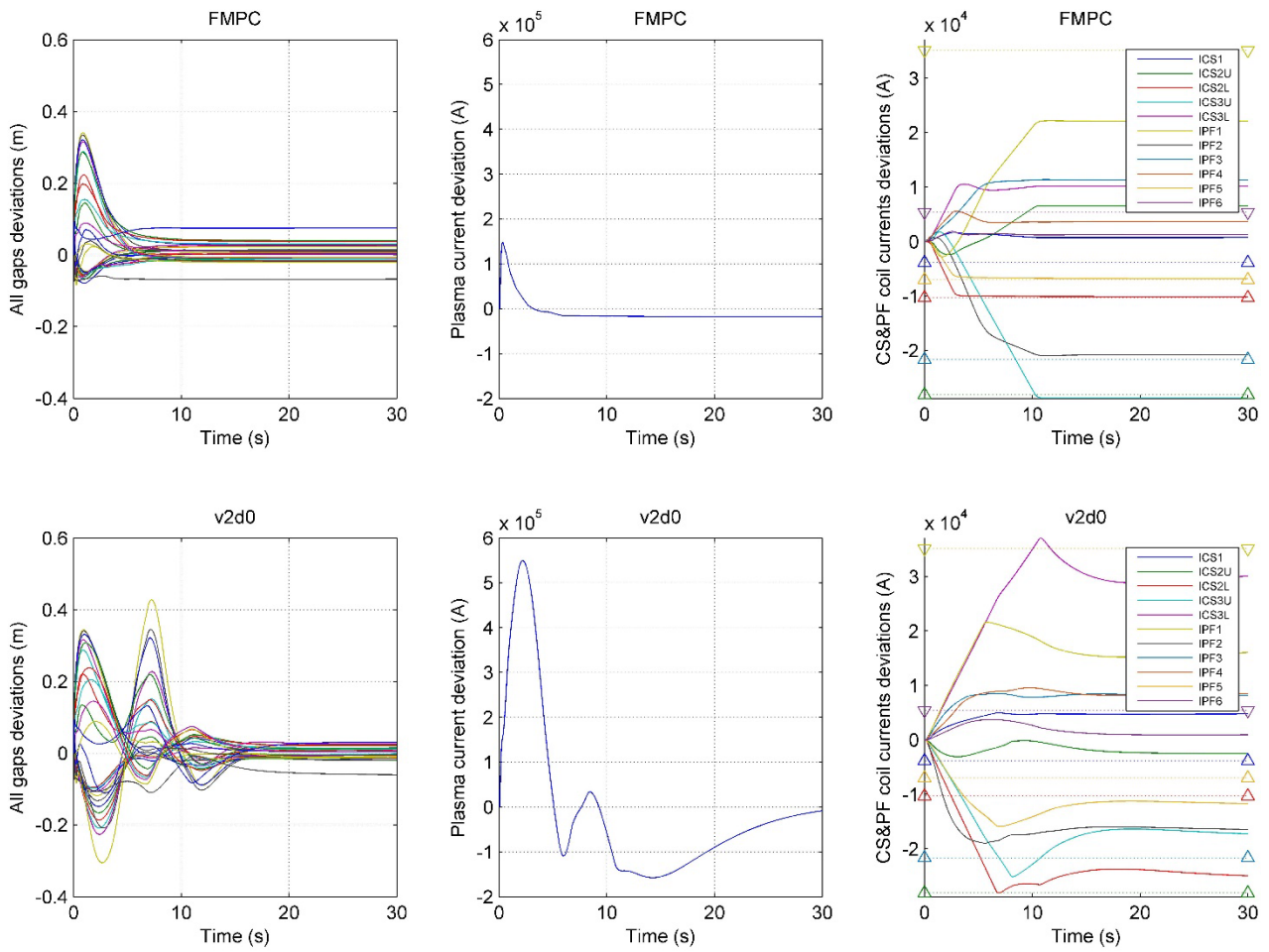


Fig. 3. Simulation performance comparison between the MPC PCSC (top) and the reference CREATE v2d0 scheme (bottom): minor disturbance at $t = 520$ s. Left: $\delta \mathbf{g}$, centre: δI_p , right: $\delta \mathbf{I}_{PF}$ (dotted lines: constraints, with triangles marking their directions)